energies

MDPI

Article

Hybrid Control Switching Technology for LLC Resonant Converter

Jie Zhang and Zhixiao Cai *

School of Electrical and Electronic Engineering, Hubei University of Technology, Wuhan 430070, China; zjmato@163.com

* Correspondence: 15827343909@163.com; Tel.: +86-158-2734-3909

Abstract: Aiming at the problem of the circuit operating frequency changing beyond the regulation range and zero switching not being guaranteed when the input voltage range of the LLC resonant converter is large, a hybrid control technology with a variable structure and variable mode is proposed in this paper to realize the wide input range of the LLC resonant converter. Depending on the input voltage range, this technology can ensure the frequency range of the circuit and meet the realization conditions of zero voltage switching (ZVS) in different modes. The test results show that the circuit can control the frequency at 0 kHz~200 kHz, the phase shift range is 0~2π/5, the maximum voltage gain multiple is 3.3 times, and the control mode is three PWM hybrid switching control.

Keywords: LLC resonant converter; wide input range; hybrid control; voltage gain

1. Introduction

LLC resonant converters are widely used because of their advantages of high efficiency and low electromagnetic interference. But when the input voltage range of LLC resonant converters is too large, the operating frequency of the circuit changes beyond the adjustment range, and the realization condition of zero voltage switching cannot be guaranteed. Therefore, it is very important to control LLC resonant converters with different input voltage ranges.

Domestic and foreign scholars have carried out relevant research in the field of LLC resonant converters. Professor Pan Jian, the first author of reference [1], proposed a fixed-frequency PWM hybrid bridge dual LLC resonant converter. Compared with the traditional LLC converters, different topological forms always work at the resonant frequency point, the corresponding switching frequency range is reduced, and the voltage gain is 2 times, but the efficiency is not high. Professor Li Changyun, the first author of reference [2], proposed a high-efficiency LLC-BUCK cascade resonant converter. The front-end circuit uses an LLC resonant converter and the back-end circuit uses an LM20343-based buck converter to realize the soft switching characteristics of the LLC resonant circuit, reduce the electromagnetic interference of the back-end input voltage, and ensure the voltage wide gain and high efficiency. But the hardware cost is high; Professor Shi Yongsheng, the first author of reference [3], proposed a method combining variable-frequency doubling technology and Burst control mode to widen the input voltage range and improve efficiency, but the circuit structure was too complicated.

Similarly, reference [4] was the first network study performed in 2024. Professor Zhang Jie, the first author of reference [4], proposed three different control strategies based on the variable mode interleaved parallel LLC resonant converter. In low-voltage applications, the converter works in the secondary parallel mode, and the output voltage can cover the range of 50~80 V combined with frequency conversion modulation. In high-voltage applications, the converter works in series mode on the secondary side, and the output voltage can cover the range of 100~150 V combined with frequency conversion modulation, but in this study [4], there is only a voltage gain multiple of 3 times, the input voltage range

check for updates

Citation: Zhang, J.; Cai, Z. Hybrid Control Switching Technology for LLC Resonant Converter. *Energies* **2024**, *17*, 6250. https://doi.org/10.3390/en17246250

Academic Editor: Michael Negnevitsky

Received: 17 October 2024
Revised: 1 December 2024
Accepted: 2 December 2024
Published: 11 December 2024

Copyright: © 2024 by the authors. Licensee MDPI, Basel, Switzerland. This article is an open access article distributed under the terms and conditions of the Creative Commons Attribution (CC BY) license (https://creativecommons.org/licenses/by/4.0/).

is not wide enough, the circuit structure is too complex, and the efficiency is low. SUN X, the first author of reference [5], proposed a two-bridge LLC resonant converter with an auxiliary switch, which adopts fixed-frequency PWM control and changes the effective input voltage of the resonator by adjusting the duty cycle of the auxiliary switch tube to achieve the stability of the output voltage. The topology can achieve soft switching in the full-load range. However, the normalized gain of this topology can only be adjusted to between 0.5 and 1, and the gain range is still limited. Some scholars have studied the two-stage converter. Professor Zhou Guohua, the first author of reference [6], proposed a Buck–Boost+LLC active booster rectifier converter, in which the Boost bridge arm is multiplexed with the LLC bridge arm, which can reduce the number of switch tubes and enable all switch tubes to achieve soft switching. Although the cascade structure can obtain a wide gain range, the overall efficiency is low. WANG W, the first author of reference [7], proposed a dynamic control method for research on the mode switching of LLC resonant convertors. The integration link is properly initialized at the beginning and end of mode switching to realize the flat sliding mode switching of LLC resonant converters, which can effectively broaden the gain range. However, the controller design is rather complicated. It is not conducive to the realization of a universal engineering application.

In summary, although LLC can achieve high voltage gain, it has the following disadvantages: (1) The multiple of the multistage converter to increase the gain is limited. (2) The control technology of LLC resonant converters is relatively complex. (3) The working efficiency of the circuit is not high enough.

Guo Chen, the first author of [8], proposed a variable-mode modulation strategy. The strategy consists of two modes: the traditional frequency modulation mode, which only adjusts the frequency, and the compound modulation mode, which adjusts both the frequency and the duty cycle. Inspired by the variable mode modulation strategy in literature [8], this paper adopts three variable mode control methods to control the output voltage. Xiaoyun Chen, the first author of reference [9], designed a DC/DC step-down half-bridge series resonant converter based on Saber. The half-bridge LLC circuit uses UC3863 as the control chip, samples the output voltage and current through a feedback loop, and drives the MOSFET tube through an isolated pulse transformer. DC/DC circuit uses a half-bridge series resonant circuit, the battery provides 48 V down to 15 V, 5 V two voltages, which can be seen the importance of MOSFET, so this paper uses MOSFET tube as a driver. Aiming at the unstable characteristics of soft switch of LLC resonant converter under variable load conditions, Dangshu Wang, the first author of reference [10], deduced the soft switch constraint conditions combined with ZVS/ZCS boundary, proposed a set of parameter optimization design methods based on full-bridge LLC resonant converter under variable load, and inspired this paper to implement ZVS with soft switch constraint conditions. Pengfei Lu, the first author of reference [11], used FHA analysis to establish a mathematical model and obtained a normalized formula, which inspired this paper to use the normalized formula for operation. Xiaofeng Sun, the first author of reference [12,13], used buck and boost converters to achieve a wide range of input voltages, but the multiple of voltage gain was not high, so this paper did not use such converters to achieve a wide range of input voltages. Dongjiang Yang, the first author of reference [14], proposed a method to achieve a wide input voltage range, which inspired the design idea of the closed-loop control part of this paper. Yubo Liu, the first author of reference [15], adopted LLC resonant converter topology for vehicle power supply in order to reduce system switching loss and improve system efficiency, which inspired this paper to adopt LLC resonant converter topology to improve circuit efficiency. Zhang, G, the first author of reference [16], proposed the control design and performance design of soft switch and double switch, which inspired the soft switch function of LLC resonant converter designed in this paper. Zhao, X, the first author of reference [17], proposed the PCB layout optimization of LLC resonant converter, which inspired the idea of using simplified circuit structure as much as possible in this paper. Yixi Liu, the first author of reference [18], proposed the application analysis and full digital control of LLC resonant converter in chargers, which inspired the circuit analysis

and control design ideas of this paper. Mengzhu Guo, the first author of reference [19], proposed a high-gain DC-DC converter based on an LLC resonant converter, which combines a full-bridge LLC resonant converter with a switching capacitor to effectively improve the gain of the converter, and thus inspired this paper to improve the voltage gain multiple by using capacitors.

Therefore, the full-bridge LLC topology is adopted in this paper, and a hybrid control technology of a variable structure and variable mode is adopted to achieve a wide range of input voltages of the converter circuit. Under different voltage ranges, three different working modes, full-bridge frequency conversion, full-bridge phase shift, and half-bridge frequency conversion, are adopted, respectively, which can ensure the frequency range and the realization conditions of ZVS.

The reason why only MOSFET switch tubes are used in the LLC topology is that the driving voltage of MOSFET used in this paper is lower than that of IGBT, the switching speed is fast, and it has soft switching characteristics, which can adapt to a wide load range and improve the reliability of the circuit. In addition, MOSFET is a voltage-driven device with high input impedance. Compared with current-driven BJT and IGBT, the MOSFET drive current is smaller, which reduces the power consumption and complexity of the drive circuit, and also makes the control circuit design easier. And MOSFET also has the following advantages:

1. Low switching loss: The switching loss of the MOSFET is relatively low when the MOSFET performs the switching operation. Especially in the LLC topology, under certain load conditions, the on–off loss of the MOSFET can be reduced to almost zero, which makes the overall switching loss very low.
2. High-frequency application capability: MOSFETs are suitable for high-frequency applications, and LLC topologies are also commonly used in high-frequency environments. The high-frequency characteristics of MOSFETs help to further reduce switching losses, thus helping to reduce the size of passive devices.
3. No trailing current: Compared with IGBTs, MOSFETs do not have a trailing current when they are turned off, which makes the MOSFETs' switching loss much lower than that of IGBTs. In an LLC topology, this is especially important because it helps achieve lower overall switching losses.
4. Short body diode recovery time: The LLC topology requires that the parasitic body diode reverse recovery time of the power switch tube is very short. MOSFETs typically have short bulk diode recovery times, which helps meet this requirement for LLC topologies.

These advantages make MOSFETs an ideal switching tube choice in LLC topologies.

2. Work Mode Analysis

The topology structure of the full-bridge LLC resonant converter adopted in this paper is shown in Figure 1.

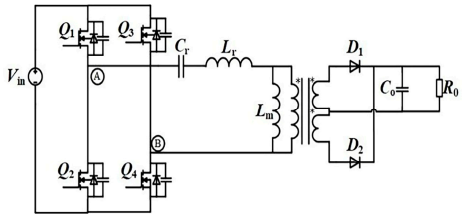

Figure 1. Topology of full-bridge LLC resonant converter.

As can be seen from Figure 1, V_{in} is the input voltage, Q_1~Q_4 is the MOSFET switching tube, C_r is the resonant capacitor, L_r is the resonant inductor, L_m is the excitation inductor, D_1 and D_2 are the rectifier diode, C_0 is the output filter capacitor, and R_0 is the output resistance.

2.1. Full-Bridge Frequency Conversion Mode

The steady-state waveform in full-bridge frequency conversion mode is shown in Figure 2.

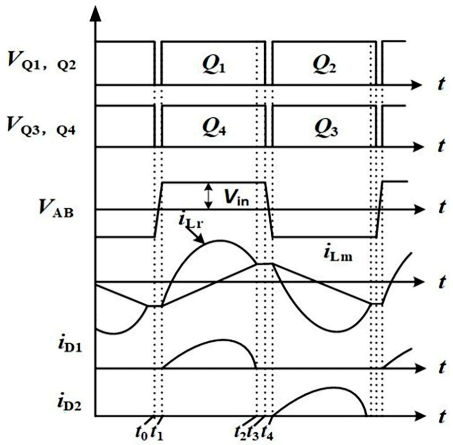

Figure 2. Steady-state waveform in full-bridge frequency conversion mode.

As can be seen from Figure 2, in full-bridge frequency conversion mode, the switch tube Q_1 and Q_4 drive signals are the same, the switch tube Q_2 and Q_3 drive signals are the same, and the Q_1 and Q_2, Q_3 and Q_4 are complementary, respectively. Since the second half-period of the full-bridge LLC variable-frequency steady-state waveform is symmetrical with the first half-period, the working mode of the half-period is analyzed [8]. The analysis of different switching modes is as follows:

(1) In switching mode 1 [t_0~t_1], the circuit diagram is shown in Figure 3.

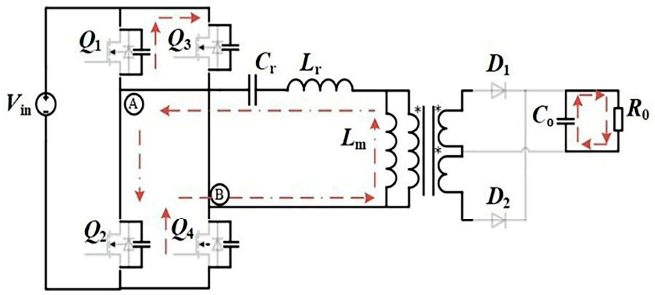

Figure 3. Circuit diagram of switching mode 1.

As can be seen from Figure 3, all the switching tubes are turned off, the junction capacitors of Q_1 and Q_4 begin to discharge, and the junction capacitors of Q_2 and Q_3 begin to charge, preparing for the zero-voltage opening of Q_1 and Q_4. At this time, the secondary side of the transformer is isolated from the primary side, and the output capacitor provides energy.

(2) Switching mode 2 [t_1~t_2]: the circuit diagram is shown in Figure 4.

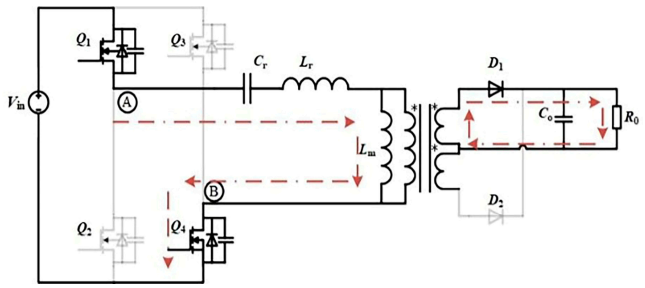

Figure 4. Circuit diagram of switching mode 2.

As can be seen from Figure 4, by switching the tube Q_1 and Q_4 zero voltage conduction, at this stage, the resonant current i_{Lr} and excitation current i_{Lm} are not equal, the difference in inductance energy is transmitted to the transformer side, the rectifier diode D_1 is switched on, and the excitation inductance L_m is clamped and does not participate in resonance. Therefore, the excitation current i_{Lm} changes linearly.

The equivalent circuit diagram of the resonator at this stage is shown in Figure 5.

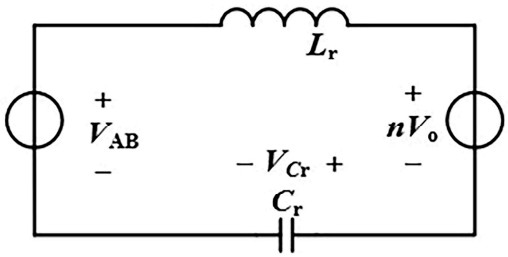

Figure 5. Resonator equivalent circuit diagram of switching mode 2.

Let $a = t - t_1$, $b = V_{in} - nV_o$, V be the peak voltage, v is the voltage change, I be the peak current, and i be the current change. After writing the circuit equation under the switching mode and performing a Laplace transform, the expressions of resonant current i_{Lr}, excitation current i_{Lm}, and resonant capacitance voltage v_{Cr} are obtained as follows:

$$i_{Lr}(t) = -I_m \cos \omega_r a + [(b - V_{Cr}(t_1)] \cdot \frac{1}{Z_r} \sin \omega_r a \tag{1}$$

$$v_{Cr}(t) = -I_m Z_r \sin(\omega_r a) + b - [b - V_{Cr}(t_1)] \cdot \cos(\omega_r a) \tag{2}$$

$$i_{Lm}(t) = \frac{nV_o}{L_m}(t - t_1) - I_m \tag{3}$$

where I_m is the peak value of excitation inductance current; ω_r is the resonant angular frequency of the resonant inductor and the resonant capacitor, which is called the resonant angular frequency, $\omega_r = 1/\sqrt{L_r C_r}$, and Z_r is the characteristic impedance, where $Z_r = \sqrt{L_r C_r}$.

(3) Switching mode 3 [t_2~t_3]: its loop diagram is shown in Figure 6:

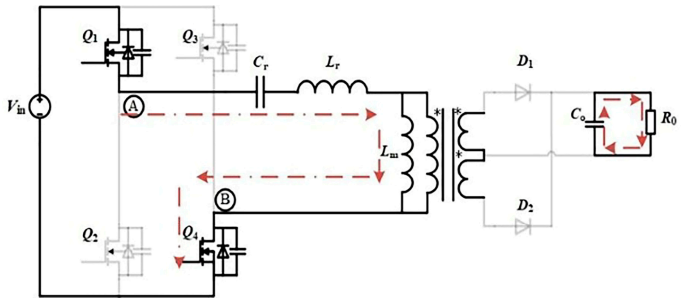

Figure 6. Circuit diagram of switching mode 3.

As can be seen from Figure 6, at this stage, Q_1 and Q_4 are still on, but the resonant current i_{Lr} and the excitation current i_{Lm} are equal, the excitation inductance L_m participates in the resonance, the rectifier diode is turned off with zero current, and the output capacitor provides energy. The equivalent circuit diagram of the resonator is shown in Figure 7. According to the equivalent circuit list of the resonator, the circuit equation under the switching mode is written and a Laplace transform is performed to obtain the expressions of i_{Lr}, i_{Lm}, and v_{Cr}, as follows:

$$i_{Lr}(t) = I_m \tag{4}$$

$$v_{Cr}(t) = V_{Cr}(t_2) + I_m(t - t_2)/C_r \tag{5}$$

$$i_{Lm}(t) = I_m \tag{6}$$

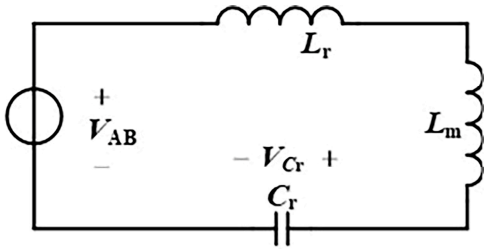

Figure 7. Resonator equivalent circuit diagram of switching mode 3.

(4) Switching mode 4 [t_3~t_4]: the circuit diagram is shown in Figure 8.

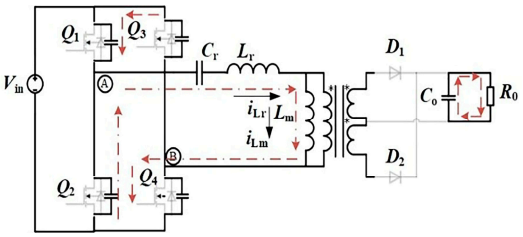

Figure 8. Circuit diagram of switching mode 4.

As shown in Figure 8, the switching tube Q_1 and Q_4 are turned off and enter the dead zone, the junction capacitors of Q_1 and Q_4 begin to charge, and the junction capacitors of Q_2 and Q_3 begin to discharge, preparing for zero-voltage opening.

According to the analysis of the operating mode, the converter has two resonant frequencies, namely, the first resonant frequency f_r of the resonant inductor L_r and the resonant capacitor C_r; and the second resonant frequency f_m of the resonant inductor L_r, the excitation inductor L_m, and the resonant capacitor C_r. Its expression is as follows:

$$f_r = \frac{1}{2\pi\sqrt{L_r C_r}} \tag{7}$$

$$f_m = \frac{1}{2\pi\sqrt{(L_r + L_m)C_r}} \tag{8}$$

The voltage gain M, quality factor Q, and equivalent resistance R_{eq} of the full-bridge LLC resonant converter in frequency conversion mode are as follows:

$$M = \frac{1}{\sqrt{\left[1 + \frac{1}{m} \cdot \left(1 - \frac{1}{f_{sn}^2}\right)\right]^2 + Q^2\left(f_{sn} - \frac{1}{f_{sn}}\right)^2}} \tag{9}$$

$$Q = \sqrt{L_r/C_r}/R_{eq} \tag{10}$$

$$R_{eq} = 8n^2R/\pi^2 \tag{11}$$

In Formulas (1)–(11), the inductance ratio $m = L_m/L_r$ and the normalized frequency $f_{sn} = f_s/f_r$, where f_s is the operating frequency of the circuit, n is the transformer ratio; that is, the transformer turns ratio, and R is the output resistance. Let m be the inductance ratio, that is, the ratio of excitation inductance to resonant inductance. A suitable inductance ratio can make the circuit have high efficiency and improve the adaptability and stability of the system.

2.2. Full-Bridge Phase Shift Mode

The LLC resonant converter under full-bridge phase shift is shown in Figure 1. Different from the modes analyzed above, the driving signal of the switching tube is no longer fixed with alternating complementary conduction, in which Q_1 and Q_2 constitute the lead-

ing arm and Q_3 and Q_4 constitute the lagging arm. Under constant frequency phase shift, the lagging bridge arm lags behind the leading bridge arm by a phase shift Angle θ. By changing the size of the phase shift Angle, the effective voltage of the resonator is changed to adjust the output voltage. The working waveform in full-bridge phase shift mode is shown in Figure 9.

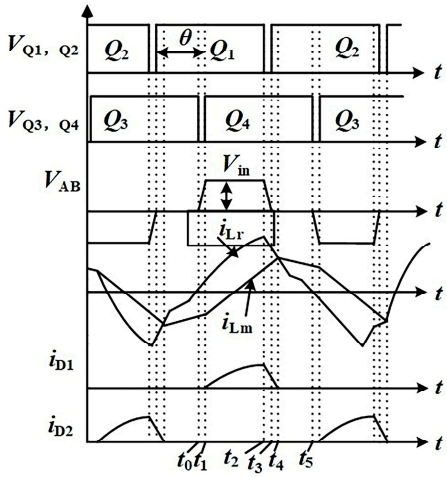

Figure 9. Working waveform diagram in full-bridge phase shift mode.

Figure 9 is the schematic diagram of the operating waveform of the LLC circuit in the phase shift control mode. The half-cycle of the full-bridge fixed-frequency phase shift control mode is analyzed. Compared with the full-bridge frequency conversion mode, the working state of switching mode 2 [t_1~t_2] is the same. However, the switching modes [t_2~t_3], [t_3~t_4], and [t_4~t_5] are different from the switching modes in the full-bridge variable-frequency control mode, and these three modes are analyzed.

(1) Switching mode 5 [t_2~t_3]: the circuit diagram is shown in Figure 10.

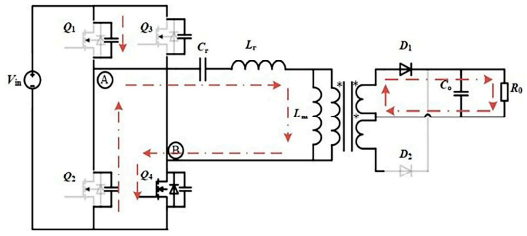

Figure 10. Circuit diagram of switching mode 5.

As can be seen from Figure 10, at t_2, Q_1 is off, and Q_4 is still on. In this stage, the junction capacitors of Q_1 and Q_2 charge and discharge each other, providing ZVS conditions for Q_2. At this stage, the voltage of the excitation inductor L_m is clamped, does not participate in resonance, and the energy is transmitted to the secondary side.

(2) Switching mode 6 [t_3~t_4]: the circuit diagram is shown in Figure 11.

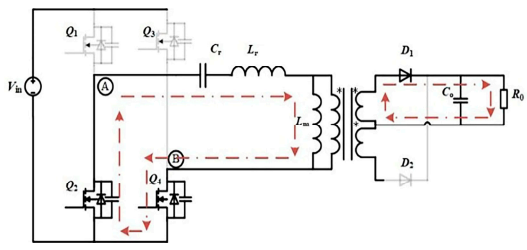

Figure 11. Circuit diagram of switching mode 6.

As can be seen from Figure 11, at t_3 moment, Q_2 is switched on with zero voltage, and the excitation inductance L_m voltage is clamped and does not participate in resonance. The cavity voltage $V_{AB} = 0$. The equivalent circuit diagram of the resonator is shown in Figure 12. Let $c = t - t_3$, $d = -nV_o - V_{Cr}(t_3)$. The expressions of i_{Lr}, i_{Lm}, and v_{Cr} are obtained by writing the circuit equation and performing a Laplace transform as follows:

$$i_{Lr}(t) = I_{Lr}(t_3)\cos(\omega_r c) + d\frac{1}{Z_r}\sin(\omega_r c) \tag{12}$$

$$v_{Cr}(t) = Z_r I_{Lr}(t_3)\sin(\omega_r c) + (-nV_o) - d\cos\omega_r c \tag{13}$$

$$i_{Lm}(t) = \frac{nV_o}{L_m}(t - t_1) - L_m \tag{14}$$

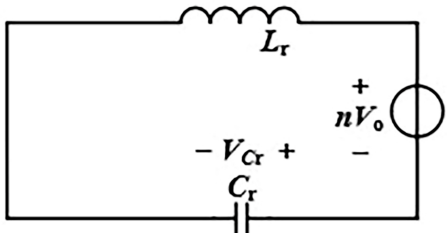

Figure 12. Resonator equivalent circuit diagram of switching mode 6.

(3) Switching mode 7 [t_4~t_5]: the circuit diagram is shown in Figure 13.

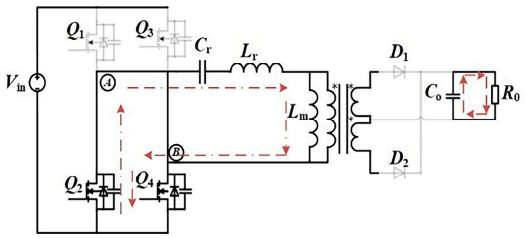

Figure 13. Circuit diagram of switching mode 7.

As shown in Figure 13, at the t_4 moment, the resonant current i_{Lr} and the excitation current i_{Lm} are equal, the excitation inductance i_{Lm} participates in the resonance, the rectifier diode is turned off with zero current, and the energy is provided by the output capacitor. The expressions of i_{Lr}, i_{Lm} and v_{Cr} at this stage are the same as those in Formulas (12)–(14).

From the above switching mode analysis, it can be seen that the full-bridge phase-shifting operation mode is equivalent to the alternating operation of two half-bridge LLC converters. The larger the phase shift Angle, the smaller the effective input voltage of the resonator, and the voltage regulation can be realized at a fixed switching frequency.

In the control of AC circuits, ωt represents the phase of the waveform at any time, and the phase shift Angle θ determines the occurrence time of the trigger signal within the waveform period. The specific expression is $\theta = \omega t + \varphi$, where θ is the phase shift Angle, indicating the phase shift of the waveform at a certain time relative to a reference point. ω is the angular frequency, representing the Angle the waveform is rotated per second, and is related to the frequency f by $\omega = 2\pi f$. t represents the time elapsed for the waveform change. φ is the initial phase, representing the phase shift of the waveform at $t = 0$.

Control method of phase shift Angle θ: The voltage set value minus the actual voltage value is calculated as the voltage error value, and the voltage error value is obtained by a PI operation, and the phase shift duty ratio is converted into delay time. The initial PWM driving signal (that is, the PWM signal of Q_1 tube) is delayed to obtain the PWM signal of the Q_2 tube. The PWM signal of the Q_4 tube is complementary to the PWM of the Q_1 tube. The PWM signal of the Q_3 tube and PWM of the Q_2 tube are complementary, and the

final drive signal is obtained by adding a dead zone to the drive signal through the delay conduction module, thus generating the phase shift Angle θ.

When the phase shift Angle is 0, the cavity voltage is consistent with the full-bridge frequency conversion, and the fundamental wave component expression of V_{AB} is as follows:

$$V_{AB} = \frac{4}{\pi} V_{in} \sin(\omega t) \tag{15}$$

The valid value is $\frac{2\sqrt{2}}{\pi} V_{in}$.

When the phase shift Angle is not 0, the fundamental wave component is

$$V_{AB} = \frac{2 \cdot (1 + \cos\theta)}{\pi} V_{in} \tag{16}$$

The DC gain under full-bridge phase shift can be obtained as

$$M = \frac{1}{2n} \cdot \frac{1 + \cos\theta}{\sqrt{\left[1 + \frac{1}{m} \cdot \left(1 - \frac{1}{f_{sn}^2}\right)\right]^2 + Q^2 (f_{sn} - \frac{1}{f_{sn}})^2}} \tag{17}$$

2.3. Half-Bridge Frequency Conversion Mode

When the full-bridge frequency conversion control and full-bridge phase shift control cannot meet the voltage gain, the converter is switched to the half-bridge frequency conversion control mode, the circuit of which is shown in Figure 14. When the LLC resonant converter is in the half-bridge frequency conversion mode, the switch tube Q_4 is always on, and the switch tube Q_1 and Q_2 are alternately on.

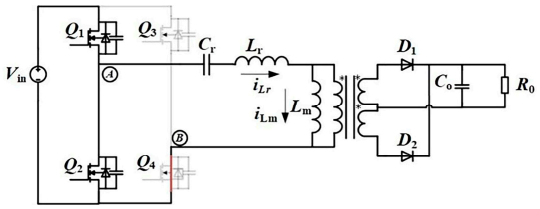

Figure 14. Circuit diagram in half-bridge frequency conversion mode.

In the half-bridge frequency conversion control mode, the working waveform is shown in Figure 15. The operating waveform of this mode is similar to that of the full-bridge frequency conversion control, but the cavity voltage v_{AB} has a no-level state of $-V_{in}$, only V_{in}, and 0 two-level states.

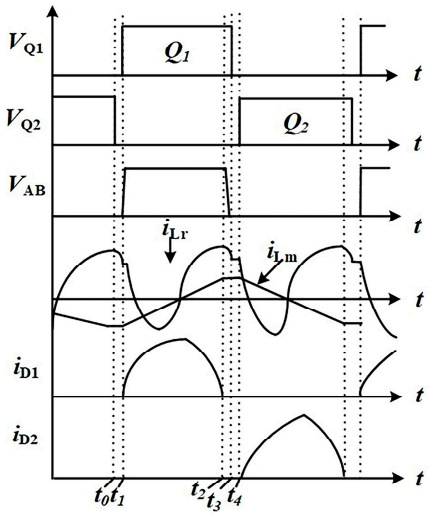

Figure 15. Working waveform diagram in half-bridge frequency conversion mode.

According to the topology of full-bridge circuits and half-bridge circuits, the voltage utilization rate of the half-bridge frequency conversion mode is half of that of the full-bridge frequency conversion mode. Therefore, the voltage gain is also half of the voltage gain of the full-bridge frequency conversion operating mode, and the analysis process is similar, so we will not go into detail here.

3. Gain Analysis

3.1. Full-Bridge Variable-Frequency Gain

The voltage gain of the full-bridge LLC resonant converter in the variable-frequency mode is the same as that of Formula (9). Figure 16 is plotted according to Formula (9).

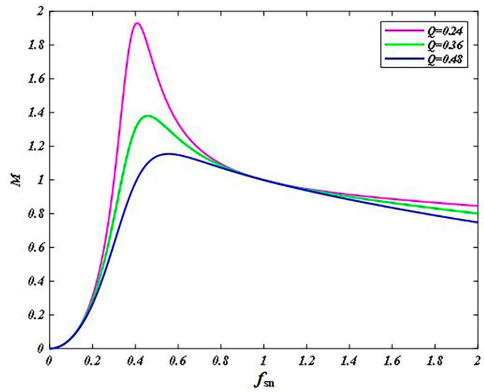

(**a**) Different Q values.

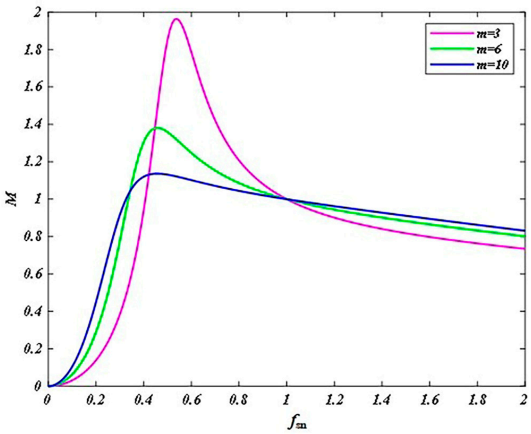

(**b**) Different m values.

Figure 16. Gain–frequency curve.

Figure 16a shows the gain–frequency curve under different Q values when m = 6. It can be seen from the figure that when m is constant, the smaller the Q value, the wider the gain range, and the steeper the gain curve. On the left side of the peak gain, the voltage gain increases rapidly with the increase in frequency, and on the right side of the peak gain, the voltage gain decreases gradually with the increase in frequency. When the normalized frequency is equal to 1, the normalized voltage gain under different Q values is equal, and both are 1. Figure 16b shows the gain–frequency curve under different m values when Q = 0.36. It can be seen from the figure that when Q is constant, the smaller m is, the larger the gain range is, and the steeper the gain curve is. When the normalized frequency is 1, the normalized voltage gain under different m values is 1. And when the normalized frequency is greater than 1, the gain curve tends to be flat, and the frequency's ability to adjust the gain becomes weak.

When m = 6, the test finds that the performance and efficiency of the circuit can reach its optimum, so the value of m is selected as 6, and the value of m under other control

methods is the same. The gain–frequency curves under different Q values are plotted, as shown in Figure 16a.

As can be seen from Figure 16a, when m is constant, the smaller the Q value, the wider the gain range. On the left side of the peak, the voltage gain increases rapidly with the increase in frequency, which is not the working region; on the right side of the peak, the voltage gain gradually decreases as the frequency increases, and the working area is also in the ZVS region. When the normalized frequency is near 1, the voltage gain under different Q values is equal.

According to the analysis of the gain–frequency curve in Figure 16, a smaller m value can obtain a wider voltage gain range, but a smaller m value also means that the excitation inductance is smaller, resulting in an increase in the excitation current and an increase in the loss of magnetic components. Similarly, a smaller Q value can also obtain a wider voltage gain range. However, according to Equation (10), it can be seen that a smaller Q value is also accompanied by a smaller characteristic impedance $Z_r = \sqrt{L_r/C_r}$, resulting in an increase in the resonant current peak value, which increases the device stress and is not conducive to the design of magnetic components. Therefore, it is necessary to select the appropriate m and Q values according to the expected peak gain.

The fixed quality factor Q = 0.36 is chosen because Q = 0.36 can improve the performance of the circuit and improve the stability of the circuit, so the value of Q under the other control methods is the same.

The gain–frequency curves under different values are drawn, as shown in Figure 16b. When Q is constant, the smaller m is, and the larger the gain range is. When the normalized frequency is 1, the gain is 1. And when the normalized frequency is greater than 1, the gain curve tends to be flat, and the frequency's ability to adjust the gain becomes weak.

It is expected that the normalized peak gain designed in this paper is 1.33. According to the two gain–frequency curves in Figure 16, when m = 6 and Q = 0.36, the gain range of the gain curve can cover the required peak gain without an excessive margin causing unnecessary loss and device stress. Therefore, m = 6 is selected. Q = 0.36 is used as the basis for the design of resonance parameters.

Fixed quality factor Q = 0.36, because Q 0.36 can improve the performance of the circuit and improve the stability of the circuit; the value of Q under other control methods is the same.

Gain–frequency curves under different m values are drawn, as shown in Figure 16b. When Q is constant, the smaller m is, and the larger the gain range is. When the normalized frequency is 1, the gain is 1. And when the normalized frequency is greater than 1, the gain curve tends to be flat, and the frequency's ability to adjust the gain becomes weak.

3.2. Full–Bridge Phase Shift Gain

The DC voltage gain of the full–bridge phase shift mode is analyzed. Figure 17 is drawn according to Formula (8). Fixed m = 6 and Q = 0.36, and gain–frequency curves under different phase shift Angles are drawn, as shown in Figure 17a.

As shown in Figure 17a, when the inductance ratio m and quality factor Q are fixed, the larger the phase shift Angle θ, the gentler the gain curve, and the narrower the gain range. At a fixed switching frequency, the voltage gain decreases as the phase shift Angle θ increases.

The gain–frequency curves under different m values are shown in Figure 17b. It can be seen from Figure 17b that when the phase shift Angle θ is fixed, the larger the m value, and the smaller the gain range. And when the normalized frequency is greater than 1, the gain curve tends to be flat, and the frequency's ability to adjust the gain becomes weak.

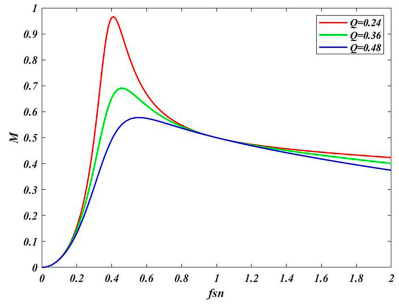

(**a**) Different phase shift Angles.

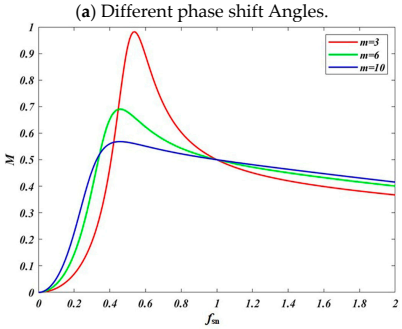

(**b**) Different m values.

Figure 17. Gain–frequency curve.

3.3. Half-Bridge Conversion Gain

Through the equivalent circuit diagram of half-bridge frequency conversion, it can be analyzed that the voltage utilization rate in the half-bridge frequency conversion mode is half of that in the full-bridge frequency conversion mode, so the voltage gain is also half of that in the full-bridge frequency conversion mode. Figure 18 is drawn based on the gain formula of half-bridge frequency conversion. The gain–frequency curves under different Q values are shown in Figure 18a.

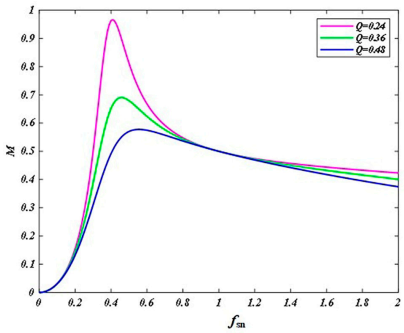

(**a**) Different Q values.

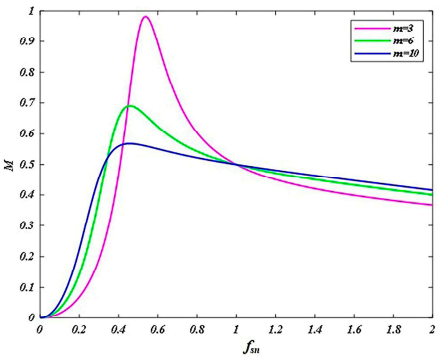

(**b**) Different m values.

Figure 18. Gain–frequency curve.

As can be seen from Figure 18a, when m is constant, the smaller the Q value, and the wider the gain range. On the left side of the peak, the voltage gain increases rapidly with the increase in frequency, which is not the working region. The voltage gain on the right side of the peak gradually decreases with the increase in frequency, and the working region is also in the ZVS region.

With $Q = 0.36$ fixed, gain–frequency curves under different values are drawn, as shown in Figure 18b.

As shown in Figure 18b, when Q is constant, the smaller m is, and the larger the gain range is. When the normalized frequency is 1, the gain is 1. And when the normalized frequency is greater than 1, the gain curve tends to be flat, and the frequency's ability to adjust the gain becomes weak. The gain expression is as follows:

$$M = \frac{1}{2} \frac{1}{\sqrt{\left[1 + \frac{1}{m} \cdot \left(1 - \frac{1}{f_{sn}^2}\right)\right]^2 + Q^2 (f_{sn} - \frac{1}{f_{sn}})^2}} \tag{18}$$

3.4. Hybrid Control Strategy Gain

Combined with the gain analysis of full-bridge frequency conversion and full-bridge phase shift, $Q = 0.36$ and $m = 6$ are selected. In the full-bridge frequency conversion mode, in order to ensure the realization of the primary side switching tube ZVS, the switching frequency should be greater than the second resonant frequency f_m, so as to obtain a voltage gain range of 3.3 times and ensure a sufficient soft switching margin. It is determined that the normalized voltage gain range under full-bridge frequency conversion is 1.33~1, and the normalized frequency range is 0.52~1 according to Equation (9).

In the full-bridge phase shift mode, the fixed switching frequency is equal to the resonant frequency, and the voltage gain is changed by adjusting the phase shift Angle. When the normalized gain is 0.67, the phase shift Angle θ can be obtained from Formula (17) as $2\pi/5$, so the limited phase shift Angle range is $0 \sim 2\pi/5$, and the normalized voltage gain in this mode is 1~0.67.

In the half-bridge frequency conversion mode, the normalized voltage gain is 0.67~0.4, which can be calculated by the half-bridge frequency conversion normalized gain analysis. The normalized frequency range is 0.52~2, and the maximum operating frequency is 200 kHz. The normalized gain obtained by the hybrid control strategy is shown in Figure 19.

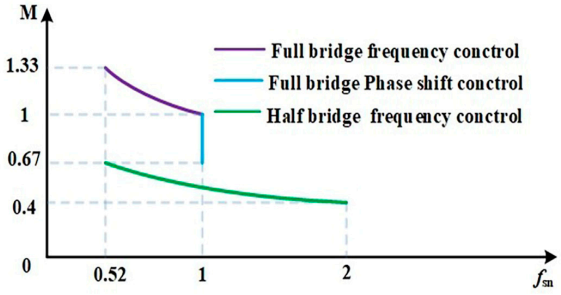

Figure 19. Gain–frequency curve of hybrid control strategy.

It can be seen from Figure 19 and the previous reasoning operations that the voltage gain of each mode is smoothly connected, and the normalized voltage gain ranges from 0.4 to 1.33. Thus, the voltage switching points of different modes in the second part of the operating mode analysis can be obtained: $V_1 = V_o/1.33n$, $V_2 = V_o/n$, $V_3 = V_o/0.67n$. Here, n is the transformer ratio, that is, the ratio of turns of the transformer. According to the normalized voltage gain range, the circuit can achieve a voltage gain range of 3.3 times. Therefore, a maximum voltage gain multiple of 3.3 times is obtained.

4. Test Verification

The system test platform is shown in Figure 20.

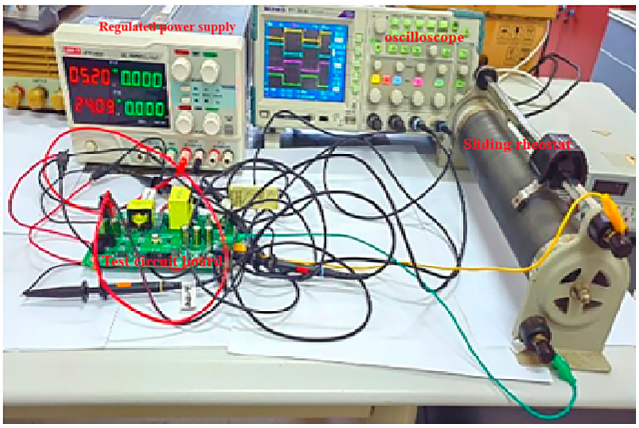

Figure 20. System test platform.

The test platform uses a TPS 2024B oscilloscope (Tektronix, Inc., Beaverton, OR, USA), 15 Ω sliding rheostat, full-bridge LLC resonant converter, and regulated power supply.

The test verification parameters are shown in Table 1.

Table 1. Test verification parameters.

Category	Numerical Value
Output voltage V_o	24 V
Resonant inductance L_r	50 μH
Resonant capacitance C_r	50 nF
Excitation inductance L_m	300 μH
Output filter capacitance C_0	470 μF

Based on the parameter settings in Table 1, the full-bridge LLC resonant converter circuit in this paper is tested and verified.

4.1. Full-Bridge Frequency Conversion Control

The current waveform of the primary side of the resonator under full-bridge frequency conversion is shown in Figure 21a. As can be seen from Figure 21a, the maximum peak value of the primary side current waveform of the resonator under full-bridge frequency conversion control is 10 A, and the lowest value is −10 A. The waveform is curved, so the oscillation occurs, which is consistent with the above theoretical analysis and the simulation run by myself, verifying the correctness of the physical test and theoretical analysis.

The secondary side current waveform of the resonator with full-bridge frequency conversion is shown in Figure 21b. The maximum value of the secondary side current of the resonator under full-bridge frequency conversion control is roughly 25 A, and the minimum value is 0 A. The waveform obtained by the test is consistent with the above theoretical analysis and the simulation run by myself, which verifies the correctness of the real test and theoretical analysis, and the proposed control method is correct to a certain extent. After testing, the output voltage of the LLC resonant converter circuit under full-bridge conversion is 24 V.

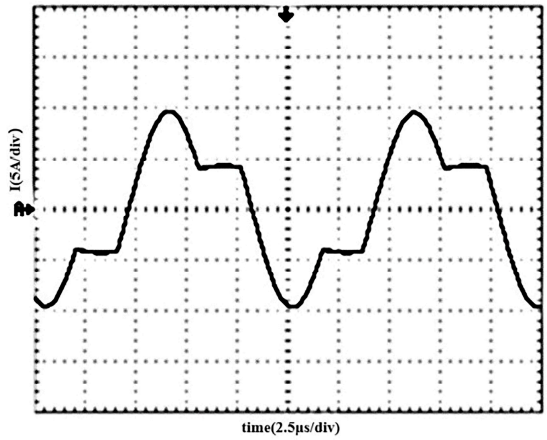

(**a**) primary side current

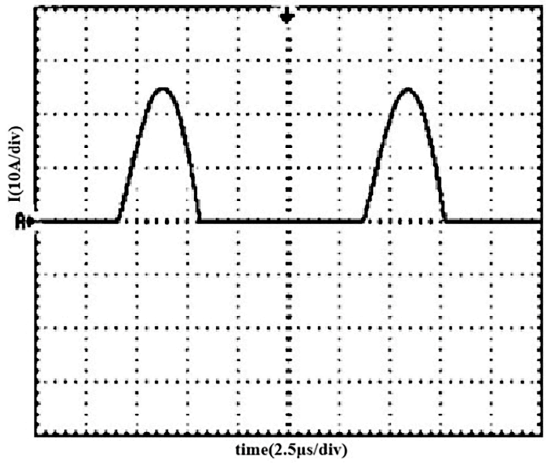

(**b**) Secondary side current

Figure 21. Resonator current waveform under full-bridge frequency conversion.

4.2. Full-Bridge Phase Shift Control

The driving voltage waveform of the circuit under full-bridge phase shift is shown in Figure 22.

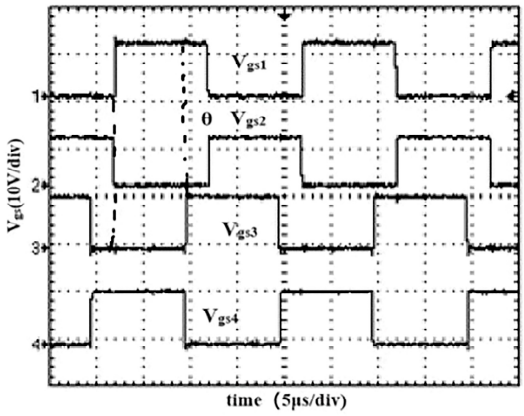

Figure 22. Waveform diagram of four MOSFET tubes under full-bridge phase shift.

As can be seen from Figure 22, V_{gs1} and V_{gs2} and V_{gs3} and V_{gs4} complement each other, and V_{gs1} and V_{gs4} have phase shift Angles θ, which verifies the full-bridge phase shift waveform in the previous theoretical analysis.

The current waveform of the primary side of the resonator with full-bridge phase shift is shown in Figure 23a.

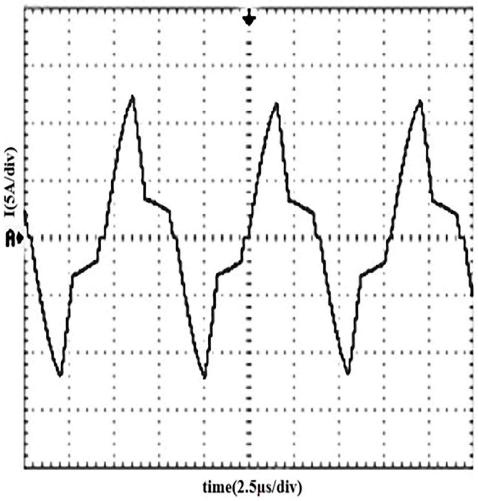

(**a**) Primary side current.

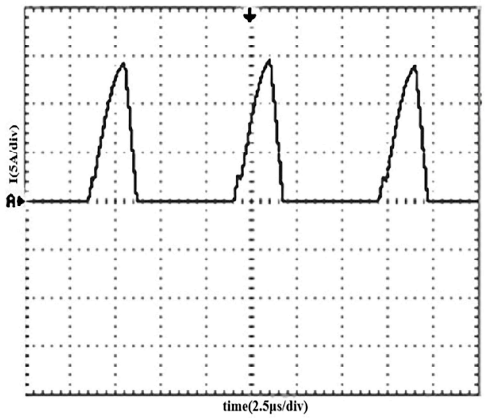

(**b**) Secondary side current.

Figure 23. Waveform diagram of resonator current under full-bridge phase shift control.

It can be seen from Figure 23a that the primary side current of the resonator under the full-bridge phase shift resonates in the ascending and descending stages, so the waveform is radian. The maximum current peak value of the primary side of the resonator is about 13 A, and the lowest value is about −13 A. The waveform of the primary side current is consistent with the above theoretical analysis and the simulation run by myself, which verifies the correctness of the real test and theoretical analysis.

The resonator subside current waveform of the full-bridge phase shift is shown in Figure 23b.

As can be seen from Figure 23b, the maximum value and minimum value of the subside current waveform of the resonator under full-bridge phase shift are roughly 14 A and 0 A, with no negative value, and resonance also occurs. The waveforms of the primary and secondary currents obtained by the experiment are consistent with the waveforms of the theoretical analysis above, and the proposed control method is correct. The waveforms of the primary and secondary side currents obtained by the experiment are consistent with the waveforms obtained by the simulation run by myself, which verifies the correctness of the physical test and theoretical analysis, and the proposed control method has a certain correctness. After testing, the output voltage of the LLC resonant converter circuit under full-bridge phase shift is 24 V.

4.3. Half-Bridge Frequency Conversion Control

The primary side current waveform of the resonator with half-bridge frequency conversion is shown in Figure 24a, and the secondary side current waveform of the resonator with half-bridge frequency conversion is shown in Figure 24b.

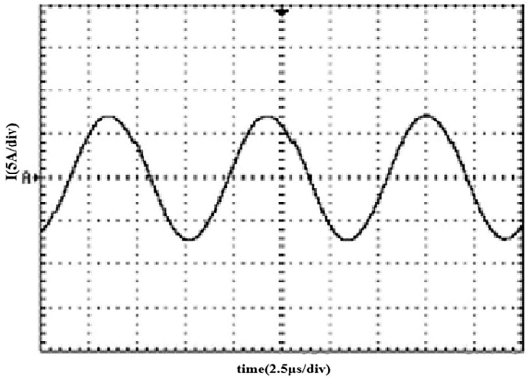

(**a**) Primary side current.

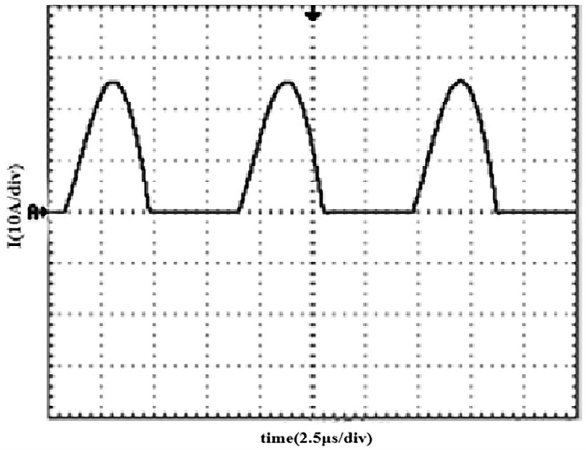

(**b**) Secondary side current.

Figure 24. Resonator current waveform under half-bridge frequency conversion.

The maximum value of the primary side current of the resonator is 7 A and the minimum value is −7 A under the half-bridge frequency conversion, and resonance occurs.

As can be seen from Figure 24, the maximum value of the primary side current of the resonator under half-bridge frequency conversion is 7 A, and the lowest value is −7 A, resulting in resonance. The maximum value of the secondary side current of the resonator is approximately 25 A, and the minimum value is 0 A. The above theoretical analysis of the waveform obtained by the experiment is consistent with that of the simulation run by myself, which verifies the correctness of the physical test and theoretical analysis, and the proposed control method has a certain correctness. After testing, the output voltage of the LLC resonant converter circuit under half-bridge frequency conversion is also 24 V.

The comparison between this paper and other literature is shown in Table 2.

Table 2. Data comparison between this paper and other studies.

Comparison Item	Literature [1]	Literature [2]	Literature [3]	Literature [20]	Literature [21]	This Text
Topological structure	Hybrid bridge double LLC	LLC-Buck cascading	Dual LLC resonant loop and voltage and current double loop control structure	Full-bridge LLC resonant converter structure	FBLLC + HBLLC structure	Hybrid bridge control structure

Table 2. *Cont.*

Comparison Item	Literature [1]	Literature [2]	Literature [3]	Literature [20]	Literature [21]	This Text
Control mode	Fixed-frequency PWM control	Fixed-frequency PWM control	Variable-frequency doubling technology is combined with Burst control mode	Two hybrid control modes	Digital control	Three PWM hybrid switching controls
Voltage gain multiple	2	1.68	2.3	2	2	3.3
Efficiency	≤90%	94.2%	87.8%	95.2%	95.8%	96%
Implemented function	ZVS	ZVS	ZVS	ZVS	ZVS	ZVS

It can be seen from Table 2. The test results in this paper are compared with those from reference [1], where only a 2× voltage gain multiple is achieved [1], and the maximum voltage gain multiple that can be achieved in this paper is 3.3 times, which exceeds the voltage gain multiple in reference [1]. The efficiency of the circuit in reference [1] is less than 90%, and the efficiency of the circuit in this paper can reach at least 96%, which is a high efficiency. The experimental results in this paper are compared with those in reference [2], and the voltage gain multiple is higher. Compared with the test results in reference [3], the circuit structure is simpler, the voltage gain multiple is higher, and the efficiency is higher. Compared with the experimental results in reference [20], the voltage gain multiple is higher and the efficiency is higher. Compared with reference [21], the experimental results in this paper show that the voltage gain multiple is higher and the efficiency is higher. It can be seen that the innovation of this paper is obvious, and it has a deeper analysis than that in other studies, so it has a certain value.

5. Conclusions

In order to solve the shortcomings of the conventional LLC resonant converter, such as the input voltage not being wide enough and the control being complicated, a hybrid switching control method of a variable structure and variable mode is proposed in this paper, which realizes the control of three working modes and the control of the output voltage. Firstly, the structure is optimized. Then, three different working modes are designed according to the different input voltage range. Finally, the experiment is verified by the test platform. The test results show that the LLC resonant converter can control the frequency range of the circuit from 0 kHz to 200 kHz, the phase shift range from 0 to $2\pi/5$, the voltage gain remains continuous and the gain multiple reaches 3.3 times, and the control mode is three PWM hybrid switching control.

Author Contributions: Conceptualization, J.Z. and Z.C.; methodology, J.Z. and Z.C.; software, Z.C.; verification, Z.C.; formal analysis, Z.C.; original draft preparation, Z.C.; visualization, Z.C. All authors have read and agreed to the published version of the manuscript.

Funding: This research received no external funding.

Data Availability Statement: The data are contained within the article.

Acknowledgments: Here, we would like to express our sincere thanks to Zhang Jie for his professional guidance in the course of this study. At the same time, we would like to thank our family and friends for their support during the study, without your help and understanding, this study could not have been completed successfully.

Conflicts of Interest: The authors declare no conflicts of interest.

References

1. Pan, J.; Song, H.; Liu, S.; Xiong, J. Research on fixed-frequency PWM controlled hybrid bridge dual LLC resonant converter. *J. Power Sources* **2024**, 1–19. Available online: http://kns.cnki.net/kcms/detail/12.1420.TM.20220224.1028.004.html (accessed on 14 September 2024).
2. Li, C.; Yang, Y.; Xu, X. A high-efficiency LLC-Buck cascade resonant converter. *Mod. Electron. Technol.* **2021**, *44*, 31–34.
3. Shi, Y.; Li, L.; Tian, W. Research on high efficiency LLC resonant converter with wide input range. *Electron Device* **2020**, *40*, 256–261.

4. Zhang, J.; Yang, L.; Zou, C.; Xiao, C.; Liu, L. Extensible wide output variable mode interleaved parallel LLC converter. *J. Power Sources* **2024**, 1–13. Available online: http://kns.cnki.net/kcms/detail/12.1420.TM.20220729.1709.004.html (accessed on 16 September 2024).
5. Sun, X.; Li, X.; Shen, Y. Dual-Bridge LLC Resonant Converter with Fixed-Frequency PWM Control for Wide Input Applications. *IEEE Trans. Power Electron.* **2017**, *32*, 69–80. [CrossRef]
6. Zhou, G.; Qiu, L.; Zhang, X. Wide Gain High Efficiency Cascade Four-Switch Buck-Boost LLC Converter. *Trans. China Electrotech. Soc.* **2024**, *39*, 1103–1115.
7. Wang, W.; Liu, Y.; Zhao, J. A Dynamic Control Method for Buck + LLC Cascaded Converter with a Wide Input Voltage Range. *IEEE Trans. Power Electron.* **2023**, *38*, 1522–1534. [CrossRef]
8. Chen, G. Variable mode modulation strategy applied to high frequency digital LLC resonant converter. *J. Power Sources* **2020**, *18*, 53–59.
9. Chen, X.; Zhang, Y. Electric vehicle LLC power supply simulation based on Saber. *Trans. China Electrotech. Soc.* **2023**, *23*, 22–23.
10. Wang, D.; Sun, L.; Dong, Z.; Jia, R.; Yang, L.; Wu, J.; Wang, X. Parameter optimization design of full-bridge LLC resonant converter under varying load. *J. Guangxi Norm. Univ. (Nat. Sci. Ed.)* **2024**, 1–13. [CrossRef]
11. Lu, P.; Wang, M.; Xie, P. Design of LED driver power based on LLC resonant converter. *J. Anhui Eng. Univ.* **2016**, *31*, 43–47.
12. Sun, X.; Shen, Y.-F.; Zhu, Y.; Liu, F.-L.; Wu, J.-J. A Boost type wide voltage range input LLC resonant converter. *Proc. CSEE* **2015**, *35*, 3895–3903.
13. Sun, X.; Qiu, J.; Li, X.; Luo, Z. An integrated Boost-Buck LLC cascade converter with a wide input voltage range. *Proc. CSEE* **2016**, *36*, 1667–1673.
14. Yang, D.; Duan, B.; Ding, W.; Song, J.; Zhang, C. A wide input voltage range LLC resonant converter with an auxiliary bidirectional switching unit. *Trans. CES* **2020**, *35*, 775–785.
15. Liu, Y.; Wang, X. Sliding mode control of on-board power LLC resonant converter for electric vehicles. *J. Electr. Mach. Control* **2020**, *24*, 131–137.
16. Zhang, G.; Zeng, J.; Yu, S.S.; Xiao, W.; Zhang, B.; Chen, S.Z.; Zhang, Y. Control Design and Performance Analysis of a Double-Switched LLC Resonant Rectifier for Unity Power Factor and Soft-Switching. *IEEE Access* **2020**, *8*, 44511–44521. [CrossRef]
17. Zhao, X.; Chen, C.-W.; Lai, J.-S. Optimization of PCB Layout for 1-MHz High Step-Up/Down LLC Resonant Converters. In Proceedings of the 2019 IEEE Applied Power Electronics Conference and Exposition (APEC), Anaheim, CA, USA, 17–21 March 2019; pp. 1226–1230.
18. Liu, Y. Research on Electric Vehicle Battery Charger Based on All-Digital Control LLC Resonant Converter. Master's Thesis, Nanjing University of Aeronautics and Astronautics, Nanjing, China, 2014.
19. Guo, M.; Chen, S.; Zheng, Z.; Guo, Y. A full-bridge LLC converter suitable for DC microgrid. *Mod. Electron. Technol.* **2024**, 1–7. Available online: http://kns.cnki.net/kcms/detail/61.1224.TN.20240328.1044.002.html (accessed on 14 September 2024).
20. Li, J.; Ruan, X. LLC resonant converter is the hybrid control strategy of the whole bridge. *J. Electrotech.* **2013**, *28*, 72–79+94.
21. Liao, Z.; Zhang, X.; You, W.; Yao, W.; Lu, Z. Variable topology LLC circuits for very wide input ranges. *J. Zhejiang Univ. (Eng.)* **2013**, *47*, 2073–2079.

Disclaimer/Publisher's Note: The statements, opinions and data contained in all publications are solely those of the individual author(s) and contributor(s) and not of MDPI and/or the editor(s). MDPI and/or the editor(s) disclaim responsibility for any injury to people or property resulting from any ideas, methods, instructions or products referred to in the content.